Editors' Suggestion

Ferroelastic domain wall motion and collective domain switching in RbSCN

V. Soprunyuk,[1] A. Tröster,[1] J. Pils,[2] W. Schranz,[2,*] I. Rychetsky,[3] A. Klic,[3] and M. A. Carpenter[4]

[1]*Institute of Materials Chemistry, TU Wien, 1060 Vienna, Austria*

[2]*Faculty of Physics, University of Vienna, Boltzmanngasse 5, 1090 Vienna, Austria*

[3]*Institute of Physics of the Czech Academy of Sciences, Na Slovance 2, 18200 Prague 8, Czech Republic*

[4]*Departement of Earth Sciences, University of Cambridge, Downing Street, Cambridge CB2 3EQ, United Kingdom*

(Received 16 March 2026; revised 21 May 2026; accepted 30 June 2026; published 17 July 2026)

Low-frequency (0.05–40 Hz) dynamic elastic measurements and resonant ultrasound spectroscopy measurements (100–600 kHz) of RbSCN were performed in the temperature region of the order-disorder improper ferroelastic phase transition at $T_c \approx 435$ K. Quite similar to KSCN, the low-frequency data show, in addition to the intrinsic phase transition anomalies, superelastic softening in the a and b directions, resulting from movements of ferroelastic domain walls under dynamic stress. However, in contrast to KSCN, a sudden discontinuous increase of Young's modulus appears in RbSCN at $T^* < T_c$, which is accompanied by a frequency-dependent damping peak. This behavior is reminiscent of a first-order phase transition. Heating RbSCN slightly above T^*, followed by subsequent cooling, removes all signs of domain wall dynamics. The results demonstrate that the anomalies in RbSCN around T^* result from collective domain switching events that are induced when the temperature-dependent critical pinning stress $\sigma_c(T)$ falls below the applied external stress σ, implying that $T^*(\sigma = \sigma_c)$. This interpretation is supported by calculations of the temperature dependences of twin boundary widths w and energies F_w, as well as the Peierls potential V_0 using a compressible pseudospin model, which leads to a critical pinning stress $\sigma_c(T)$ that is in excellent agreement with experimental values of $T^*(\sigma_c)$.

DOI: 10.1103/rmsb-fvm3

I. INTRODUCTION

Similar to other ferroics, ferroelastic materials form regions of symmetry-related long range ordered states (domains), which are separated by domain walls and which are switchable by the application of an external stress [1]. Understanding the dynamical behavior of domain walls (DWs), which is at the core of domain switching [2], is vital for the development of novel nanotechnological devices [3,4]. Ferroelastic switching as a function of external stress often occurs via jerky movement of twin boundaries (TBs) [5–8], which can trigger larger collective switching events (avalanches) [9,10], forming a typical stress-strain hysteresis [11].

Quite an extensive body of literature on DW motion, domain switching, and its influence on macroscopic susceptibilities exists [12]. Theoretical work includes Landau free energy expansions in terms of a continuous order parameter appended with terms containing the order parameter gradient [13], phase field calculations [14,15], and other computer simulations [16,17], to name only a few. The first experimental evidence that domain walls move in a jerky, collective way rather than smoothly was presented in 1919 by Barkhausen [18] for magnetic systems. The idea of elastic domain wall motion emerged gradually as experimental techniques improved and domain walls began to be treated as elastic interfaces moving in a disordered medium [19,20]. The first clear experimental demonstration of elastic domain wall dynamics was published [21] in the 1990s, showing the creep behavior of a magnetic domain wall in an ultrathin Pt/Co/Pt film driven by a magnetic field. Meanwhile, DW dynamics have been studied in a number of ferroic (ferromagnetic, ferroelectric, multiferroic) systems, showing quite universal behavior [22], in agreement with theory. However, the ac response of elastic DWs in ferroelastics (proper or improper) and its relationship with magnetic and electric DW dynamics certainly merit attention.

Here we show that crystals of the family MSCN (M = Rb, K), which exhibit an antiferrodistortive phase transition, where the order parameter is not the magnetization **M** but is given by a combination of pseudospin variables S_i ($i = 1, 2, 3, 4$) coupled to strain ε_α, exhibit quite interesting DW dynamics in response to a dynamically applied stress.

In Sec. II we review the main features of the phase transition properties of RbSCN. Section III reports on low- (0.05–40 Hz) and high- (100–600 kHz) frequency elastic measurements of RbSCN. In Sec. IV we discuss the present data by combining well-known theories of DW motion with a compressible pseudospin model. Section V concludes the paper.

II. PHASE TRANSITION IN RUBIDIUM THIOCYANATE

RbSCN crystals undergo an order-disorder improper ferroelastic phase transition (PT) at $T_c \approx 435$ K from a

*Contact author: wilfried.schranz@univie.ac.at

Published by the American Physical Society under the terms of the Creative Commons Attribution 4.0 International license. Further distribution of this work must maintain attribution to the author(s) and the published article's title, journal citation, and DOI.

TABLE I. Lattice parameters of RbSCN and KSCN.

	RbSCN	KSCN
a_t (Å)	6.9198	6.740
c_t (Å)	8.2904	7.832
a_o (Å)	6.8373	6.676
b_o (Å)	6.8859	6.691
c_o (Å)	8.0102	7.606

high-temperature tetragonal body-centered structure [23] with space group $I4/mcm$ (D_{4h}^{18}), with 2 f.u. in the primitive unit cell, to an ordered low-temperature orthorhombic space group $Pbcm$ (D_{2h}^{11}) with 4 f.u. in the unit cell (see Fig. 1 of Ref. [24]). Above T_c the SCN^- ions are head-tail disordered on average, and below T_c they order in an alternating arrangement, resulting in the loss of the centering translation $(\frac{1}{2}, \frac{1}{2}, \frac{1}{2})$. The lattice constants of the conventional tetragonal unit cell $\mathbf{a}_t = (a_t, 0, 0)$, $\mathbf{b}_t = (0, a_t, 0)$, and $\mathbf{c}_t = (0, 0, c_t)$ of RbSCN [23] and KSCN [25,26] and of the orthorhombic unit cell are presented in Table I.

Due to the symmetry reduction at the phase transition, four domain states (DSs) [27,28] are possible below T_c. DSs 1_1 and 1_2 and 2_1 and 2_2 are related by lost translations $(\frac{1}{2}, \frac{1}{2}, \frac{1}{2})$ and are separated by antiphase boundaries (APBs), and DSs 1_1 and 2_1 and 1_1 and 2_2 are related by 90° rotations and are separated by ferroelastic DWs, also known as twin boundaries. The PT properties of RbSCN were previously studied in detail using a number of experimental methods, including NMR [29], neutron scattering [30], and Raman and infrared measurements [31], as well as by molecular dynamics [32] and Monte Carlo [33] simulations.

Thermodynamic properties [29,30] of the order-disorder PT in RbSCN have been well described by a compressible pseudospin model [34], i.e., by including coupling between the pseudospin variables S_i $(i = 1, \ldots, 4)$ and the strain components ε_α of the type $\alpha_{ijk} S_i S_j \epsilon_k$. These order parameter–strain couplings result in relatively large (diplike) anomalies of the longitudinal elastic constants, as previously measured in KSCN [35–37].

Insights into the dynamical behavior of the SCN fluctuations were gained by NMR measurements [29]. The fact that the ^{87}Rb NMR line is homogeneously broadened demonstrates that the disorder is dynamic. However, the timescale τ_η of the SCN head-tail fluctuations is so slow that low-symmetry ^{87}Rb $\frac{1}{2} \rightarrow -\frac{1}{2}$ NMR angular rotation patterns are observed above T_c, implying that the high-temperature phase of RbSCN consists of a large number of orthorhombic nanodomains with lifetimes $10^{-7} < \tau_\eta < 10^{-3}$ s. Similar slow dynamics of order parameter (OP) fluctuations were also found in KSCN [38].

Diffuse neutron scattering data of RbSCN [30] showed that in the tetragonal phase the size ξ of the nanodomains increases with decreasing temperature as

$$\xi_a\,[\text{Å}] = \frac{55}{\sqrt{T - T_0}}, \quad \xi_c\,[\text{Å}] = \frac{38}{\sqrt{T - T_0}}. \tag{1}$$

Quite unusually, in the whole orthorhombic phase the correlation length is independent of temperature with $\xi_a \approx 30$ Å and $\xi_c \approx 25$ Å. For comparison, in KSCN $\xi_a = 66/\sqrt{T - T_0}$, $\xi_c = 42/\sqrt{T - T_0}$ (at $T > T_c$), and $\xi_a \approx \xi_c \approx 20$ Å(at $T < T_c$) were found [39]. Molecular dynamics calculations [40–42] of a two-dimensional KSCN model including order parameter–strain coupling of the type $\eta^2\varepsilon$ reproduce this unusual behavior. Later, it was argued [43] that inhomogeneous strains suppress the growth of the clusters below T_c. Current Monte Carlo (MC) simulations [44] using a compressible pseudospin Hamiltonian, including inhomogeneous strains, support this scenario.

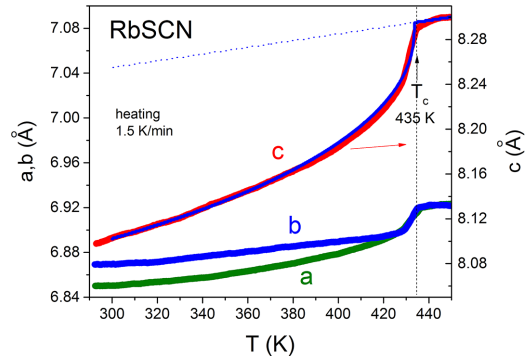


FIG. 1. Thermal expansion of RbSCN in the three directions measured with a TMA 4000 (Perkin Elmer). The measured values of the sample dimensions l_a, l_b, and l_c are normalized to the lattice parameters a, b, and c at $T_c = 435$ K.

Cooling the crystals leads to a dense network of needle-shaped ferroelastic domains. In the following we present recent dynamic elastic measurements, unveiling the dynamics of TBs of RbSCN, and compare them with results of KSCN [24].

III. DYNAMIC ELASTIC RESPONSE OF RUBIDIUM THIOCYANATE

RbSCN single crystals were grown by slow evaporation from an aqueous solution of NH_4SCN and Rb_2CO_3 by Fuith [45]. To prepare samples for TMA (thermomechanical) and DMA (dynamic mechanical) measurements, the crystals were oriented (according to the known morphological habit planes), cut with a diamond saw, and polished with diamond paste. The typical sizes of the samples were prisms of $L \approx 3$ mm and $A \approx 1.5 \times 1.5$ mm^2 for parallel plate measurements and bars of length $L \approx 2$–3 mm, thickness $t \approx 0.5$–1 mm, and width $b \approx 1$ mm for three-point bending measurements.

Figure 1 shows thermal expansion measurements of RbSCN using a TMA 4000 (Perkin Elmer). The data are normalized to the lattice parameters [23] at 435 K to obtain the temperature dependences of a, b, and c. The resulting room temperature lattice parameters agree reasonably well with those determined from x-ray scattering [23], thereby confirming the assigned orientations of the samples.

The Young's modulus Y' and $\tan\delta$ are determined by measuring the dynamic amplitude u and phase shift δ between force and amplitude in response to an applied dynamic force $F(t) = F_s + F_d \sin(\omega t)$ using a Diamond DMA (Perkin Elmer). By subsequently applying a sinusoidal oscillation of varying frequency, the dynamic elastic response is determined for a number of frequencies in a single temperature run.

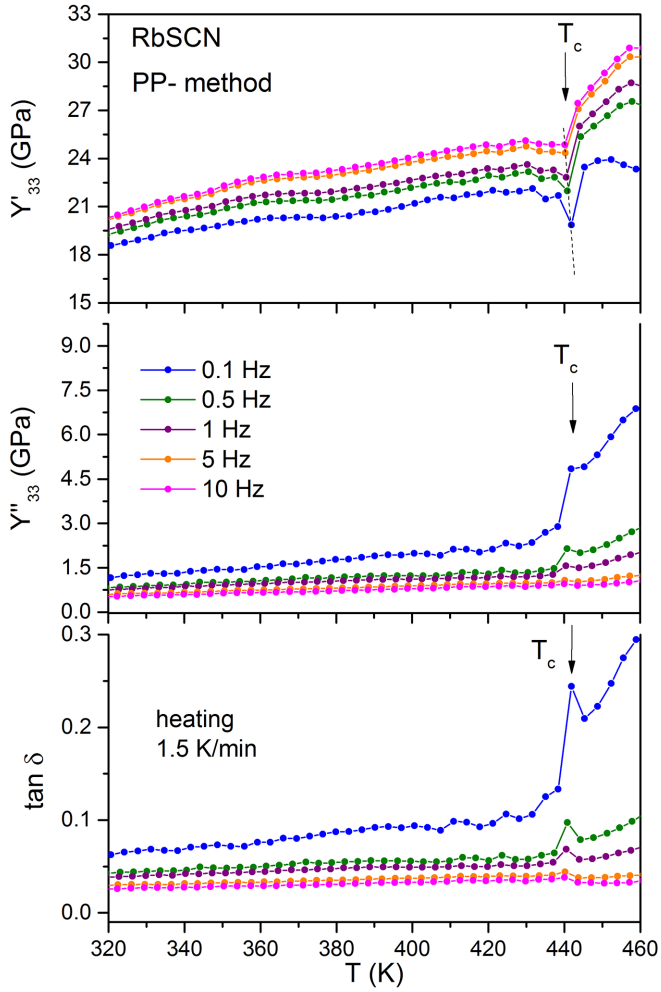


FIG. 2. Temperature and frequency dependences of Y'_{33}, Y''_{33}, and $\tan\delta$ of RbSCN, measured in the parallel plate mode with a Diamond DMA (Perkin Elmer). Different frequency curves are shifted for clarity.

Figure 2 shows the elastic response with applied stress in the c direction at frequencies between 0.1 and 10 Hz. In this direction no domain wall response is detected, as expected for this geometry. The negative dip anomaly in Y'_{33} and the peak in Y''_{33} close to T_c result from coupling terms of the type $\alpha\eta^2\epsilon$ in the Landau free energy expansion.

In a previous work [36] we showed that at T_c the decrease in the anomalies in Y'_{33} and Y''_{33} with increasing frequency (0.1–50 Hz) results from heat diffusion, i.e., a crossover from isothermal to adiabatic elastic behavior [36] when $\omega\tau_{\rm th} < 1 \rightarrow \omega\tau_{\rm th} > 1$. $\tau_{\rm th}$ is the thermal relaxation time, which is of the order of 0.01 s.

Figure 3 displays results from resonant ultrasound spectroscopy (RUS) measurements, and primary spectra were collected using the instrument described in Ref. [46]. Individual peaks in the frequency range 100–600 kHz were fit with an asymmetric Lorentzian function to determine their frequency f and width at half maximum height Δf. f^2 scales with different combinations of single-crystal elastic constants $C_{\rm el}$. Acoustic loss scales with the inverse mechanical quality factor, $Q^{-1} = \Delta f/f$. The peaks were too broad to measure at exactly the transition point, but otherwise, the results are

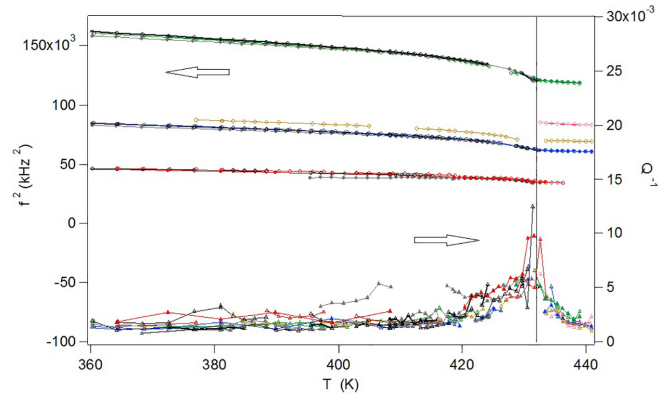


FIG. 3. Temperature evolution of $f^2 \propto C_{\rm el}$ and $Q^{-1} \propto \tan\delta$ for some selected resonances in RUS spectra of RbSCN. All resonances show similar temperature dependences.

quite clear. The transition is close to being continuous, and there is a peak in Q^{-1} at the transition point. There is no sign of any domain wall mobility, and the elastic constants $C_{\rm el} \propto f^2$ stiffen rather than showing the softening that would be expected if the order parameter were able to relax on a timescale of $\sim 10^{-6}$ s. In agreement with NMR results [29] this implies that $\tau_\eta > 10^{-6}$ s.

In contrast to the Young's modulus in the c direction, the a and b directions yield quite different behaviors at low frequencies (Figs. 4 and 5).

For stresses applied in the a or b direction, the TBs contribute to the corresponding dynamic elastic behavior quite similarly to what was observed in other multidomain ferroelastic materials [47,48]. The most striking feature is the additional anomaly around a temperature T^* markedly lower than T_c. Y' shows a discontinuous increase at T^*, which decreases with increasing frequency and is accompanied by a peak in Y'' whose magnitude also decreases with increasing frequency (Figs. 4 and 5). In contrast to the peak around $T_{\rm DW}$, the one at T^* does not shift with varying frequency. Such behavior is reminiscent of a first-order phase transition. We will discuss its origin below.

The peak at $T_{\rm DW}$ shifts to lower temperature with decreasing frequency. This shift results from the decreasing mobility of TBs with decreasing temperature as the domain wall relaxation time $\tau_{\rm DW}$ increases. The crossover from $\omega\tau_{\rm DW} < 1$ to $\omega\tau_{\rm DW} > 1$ leads to a maximum in Y''_{11} at $\omega\tau_{\rm DW} = 1$ around 380 K. Similar behavior was also found recently in KSCN [24]. However, because of the absence of any T^* anomaly in KSCN, the TB-induced softening in Y' between $T_{\rm DW}$ and T_c is clearly visible, whereas in RbSCN it is masked by processes occurring close to and above $T^* \approx 400\ K$.

To get a clue about the anomalies around T^* we heated the RbSCN crystal from room temperature to a temperature slightly above T^*, cooled it back to room temperature, and heated it again to temperatures above T_c. Figure 6 shows a typical heating-cooling-heating run at a rate of 1.5 K/min. Changing heating/cooling rates (1–5 K/min) did not change the behavior. We observe that subsequent cooling from $T > T^*$ removes all signatures of DW movement. This is most clearly demonstrated by the absence of any peaks in Y'' or $\tan\delta$ after cooling from above T^*. Stopping the first heating run at

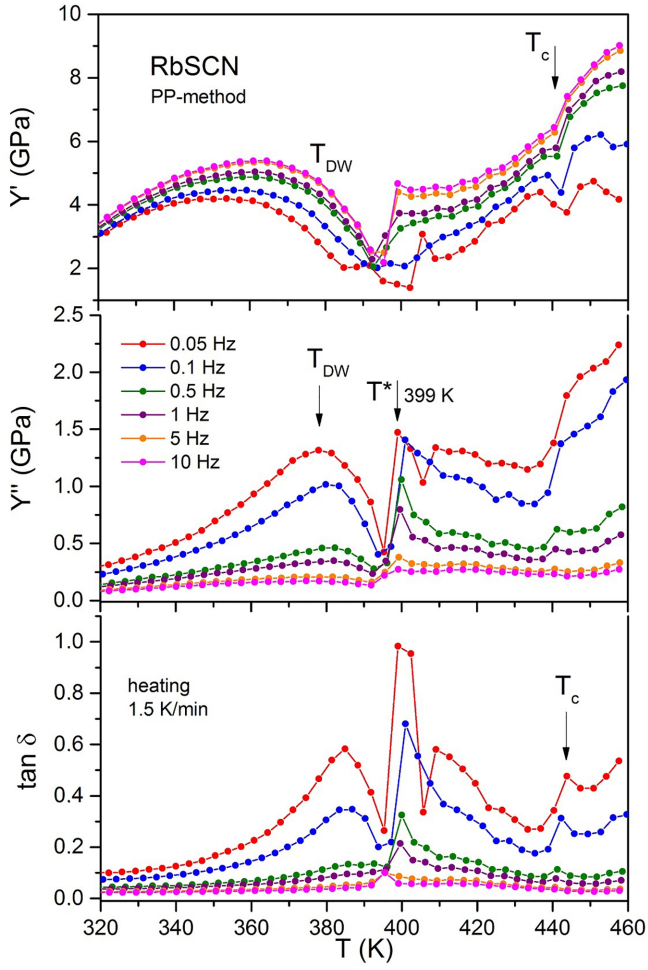


FIG. 4. Temperature and frequency dependences of Y'_{11}, Y''_{11}, and $\tan\delta$ of RbSCN, measured during heating from room temperature in the parallel plate mode with a Diamond DMA (Perkin Elmer). The stress is applied in the a direction. $T_{\rm DW}$ marks the domain freezing temperature at $\omega\tau_{\rm DW}(T) = 1$. T^* is explained in the text.

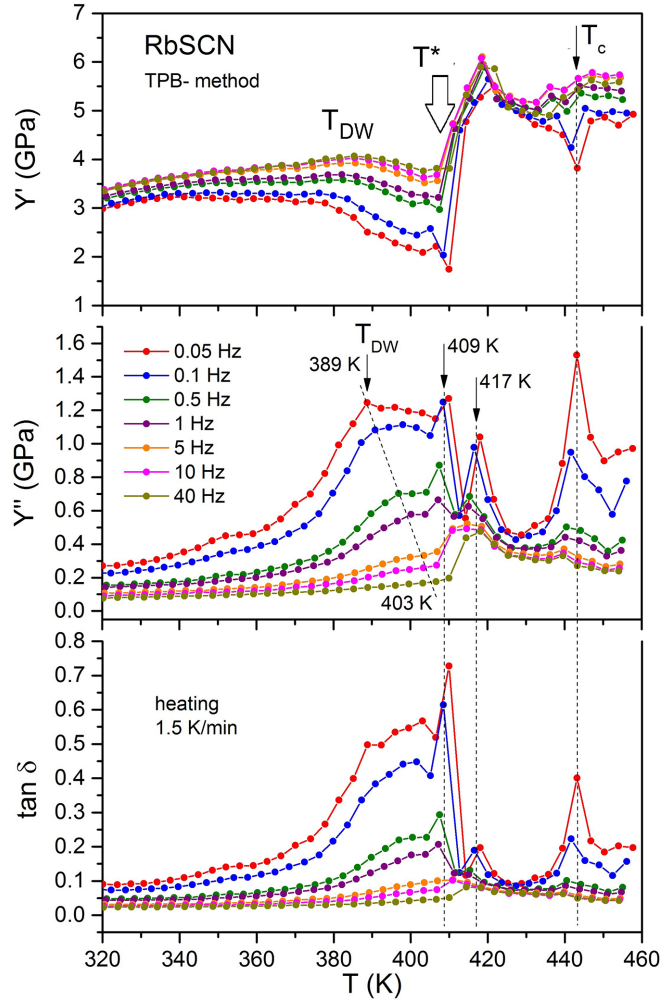


FIG. 5. Temperature and frequency dependences of Y'_{11}, Y''_{11}, and $\tan\delta$ of RbSCN, measured in three-point bending geometry with a Diamond DMA. With applied force $F = 6.4$ N and sample dimensions $L = 3$ mm, $b = 2.78$ mm, and $t = 1.21$ mm, the average (over sample thickness t) flexural stress $\sigma = 3FL/4bt^2 \rightarrow \sigma_2^* \approx 4$ MPa, and $T_2^* \approx 410$ K.

$T < T^*$ and cooling back to room temperature did not yield any anomaly; i.e., Y' is identical to the first heating curve. This suggests that the anomalies in RbSCN observed around T^* are related to correlated (avalanchelike) domain switching events in response to the applied stress in the parallel plate and three-point bending DMA measurements. Interestingly enough, T^* depends on the applied flexural stress (cf. Figs. 5 and 6).

In the following section we will describe the various contributions to the dynamic elastic response of RbSCN in its monodomain and multidomain states.

IV. DISCUSSION

A. Monodomain response

Let us start to describe the different patterns shown in Figs. 2–6. To calculate the intrinsic (due to the PT) temperature dependences of the elastic constants we use a compressible pseudospin model [34]. In the model, the anomaly in the longitudinal elastic constants is induced by the coupling terms between the order parameter η and the strains ϵ_i ($i = 1, 2, 3$), which are of the type $\alpha_i\eta^2\epsilon_i$. The corresponding expression—sometimes called the Landau-Khalatnikov (LK) contribution—can be written as [35] $C_{ij} = C_{ij}^{\infty} + \Delta C_{ij}^{\rm LK}$, with

$$\Delta C_{ij}^{\rm LK} = -\frac{\alpha_i\alpha_j T_0}{V k_B T}\frac{\eta_s^2\left(1-\eta_s^2\right)^2\left(1+A\eta_s^2\right)}{T - T_0\left(1-\eta_s^2\right)\left(1+A\eta_s^2\right)}, \qquad (2)$$

where T_0 is the stability limit of the high-temperature phase and the parameter A measures the ratio between the elastic energy and the exchange energy $J = k_B T_0$. If $A < \frac{1}{3}$, the PT is of second order; it is of first order for $A > \frac{1}{3}$, and $A = \frac{1}{3}$ corresponds to a tricritical point at T_0. For RbSCN, a value of $A \approx 0.36$ was reported [29], thus being very close to a tricritical point. For KSCN, a value of $A \approx 0.5$ was reported [35,37], implying that the PT is of first order with $T_c - T_0 \approx 3K$.

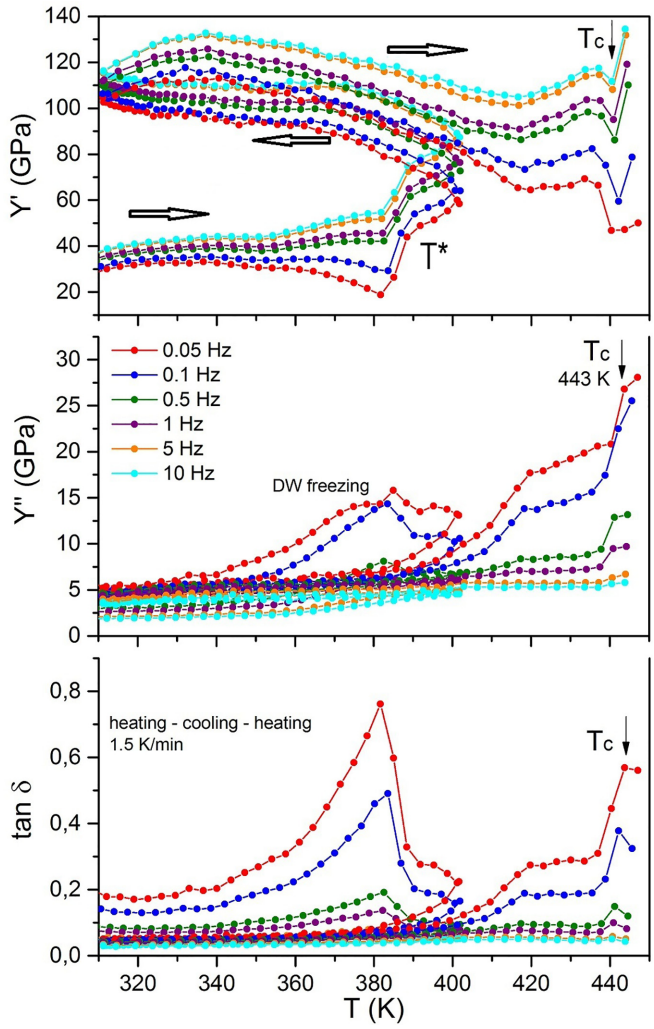


FIG. 6. Temperature and frequency dependences of Y'_{11}, Y''_{11}, and $\tan\delta$ of RbSCN, measured in three-point bending geometry with a Diamond DMA for a sequence of heating above $T^* \approx 380$ K, followed by subsequent cooling to room temperature and heating again to a temperature above T_c. With applied force $F = 9$ N and sample dimensions $L = 2$ mm, $b = 1.78$ mm, and $t = 0.51$ mm, the average (over sample thickness t) flexural stress $\sigma = 3FL/4bt^2 \rightarrow \sigma_1^* \approx 30$ MPa, and $T_1^* \approx 380$ K.

The equilibrium value η_s of the OP is calculated from the relation

$$\eta_s(T) = \tanh\left[\frac{T_0}{T}\left(\eta_s + A\eta_s^3\right)\right]. \tag{3}$$

Equation (2) holds for $\omega\tau_\eta < 1$ and $\omega\tau_{\rm th} < 1$, where τ_η is the order parameter relaxation time, which determines the timescale of OP fluctuations, and $\tau_{\rm th}$ is the thermal relaxation time, characterizing the temperature exchange between different regions in the crystal. The observed dip anomalies in the real part and the peak at T_c in the imaginary part of the Young's modulus shown in Figs. 2, 4, and 5 are typical for the LK contribution (2). The decrease in these anomalies with increasing frequency implies a crossover from $\omega\tau < 1 \rightarrow \omega\tau > 1$. The absence of any dip anomalies in $f^2 \propto C_{\rm el}$ for RUS measurements (Fig. 3) demonstrates that the order parameter cannot relax on the timescale of the strain variations (some 10^5 Hz), implying $\tau_\eta > 1/\omega \approx 10^{-6}$ s. In previous work we showed [24,37] that in such a case the anomalies can be fitted by $C_{\rm el} \propto \eta_s^2$, originating from additional $\eta^2\varepsilon^2$ terms in the corresponding Landau free energy expansion.

Quite interestingly, Q^{-1} data (Fig. 3) display peaks at all frequencies even above T_c, whereas no such precursor effects are found in the resonance frequencies which are proportional to the elastic constants. Such unusual behavior was also found recently in KSCN [24] and explained in terms of order parameter fluctuations with a rather large timescale ($\tau_\eta > 10^{-6}$s).

B. Effects of twin boundary motion

From Figs. 4 and 5 it is obvious that in contrast to the c direction (Fig. 2), Young's moduli in a and b directions are dominated by TB motion. TB motion usually leads to superelastic softening in Y', accompanied by a broad peak in Y'', whose maximum at the temperature $T_{\rm DW}$ (at $\omega\tau_{\rm DW} = 1$) shifts to higher temperatures with increasing frequency of the applied stress [47,48,50–52]. Such behavior is, indeed, found for RbSCN (Figs. 4 and 5). However, it is interrupted by a discontinuous increase of Y' at T^*, which is accompanied by a peak in Y''. The temperature T^* of the anomalies does not shift with frequency but shifts to lower temperature with increasing stress. In the following we will substantiate that the anomalies at T^* are related to domain switching.

To calculate the TB contributions to the dynamic elastic response we follow the theoretical elaborations of Refs. [12,13,54,55]. The application of an external macroscopic stress σ results in a pressure $\sigma\varepsilon_s$ applied to TBs in the ferroelastic state. This results from the strain contrast $\varepsilon_s = \varepsilon_1^h - \varepsilon_2^h$ between two adjacent ferroelastic domains, 1_1 and 2_1, and will finally result in the motion of the ferroelastic DWs. For adjacent APBs the homogeneous strains are equal on both sides, implying $\varepsilon_s = 0$, which implies that APBs cannot be moved by external stress.

Quite generally, the movement of DWs in external fields can be hindered due to pinning by various obstacles, i.e., point defects, dislocations, surface, neighboring TBs or antiphase boundaries, etc. Here we will consider the case of lattice pinning (Peierls pinning) as TBs in RbSCN and KSCN turn out to be very thin. Depending on the relation between the external stress and the strength of pinning, one can roughly distinguish two regimes of DW motion, i.e., thermally activated and nonactivated regimes. Let us recall an explanation of the two regimes [12,13].

For very thin DWs the surface energy density $F_w(z)$ of a domain wall depends on the position z of the wall center with respect to the sites of the crystal lattice (Fig. 7).

It is given as [13]

$$F_w(z) = F_w(0) + \frac{V_0}{2}\cos\left(\frac{2\pi z}{a}\right), \tag{4}$$

where V_0 is related to the pinning barrier and reads

$$V_0 = 8\pi^4 F_w(0)\left(\frac{w}{2a}\right)^3 \exp\left(-\pi^2\frac{w}{2a}\right). \tag{5}$$

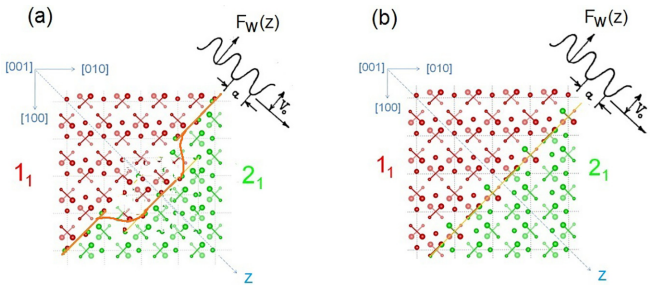


FIG. 7. Sketch of the movement of a TB segment trapped in the Peierls potential, forming a nucleus of the inverse domain. (a) A TB segment that jumped over the barrier and (b) the TB at the saddle point.

w is the DW thickness, and $F_w(0)$ is the TB energy density as calculated, e.g., from a continuous Landau-Ginzburg model [53] at $z = 0$.

The exponential dependence of V_0 on the TB thickness w leads to a very pronounced temperature dependence of a number of physical quantities. For narrow TBs with $w \approx a$, the presence of the pinning barriers prevents their motion as a whole at relatively weak external stresses, as it would require overcoming energy barriers of the order $E_B = S_0 V_0 \gg k_B T$ (S_0 is the area of the TB). In this so-called thermally activated regime $\sigma < \sigma_c$, only small segments of the TB can perform thermally activated jumps, forming nuclei of the reverse domain (Fig. 7). The crossover from the activated to the nonactivated regime [13] occurs at a critical stress of about

$$\sigma_c \approx \frac{V_0}{\varepsilon_s a}, \tag{6}$$

where $\varepsilon_s = \varepsilon_1^h - \varepsilon_2^h$ is the strain contrast between adjacent ferroelastic domains. As we show in the Supplemental Material (SM) [49], the homogeneous spontaneous strains in adjacent domains are $\varepsilon_1^h = k_1 \eta_s^2$ and $\varepsilon_2^h = k_2 \eta_s^2$. As a result, $\varepsilon_s = (k_1 - k_2)\eta_s^2 = 0.003\ \eta_s^2(T)$.

The critical stress is strongly temperature dependent (Fig. 8) through V_0 [Eq. (5)], which depends exponentially on the TB thickness $w(T)$. In Ref. [53] we calculated the TB thickness and corresponding energies for KSCN crystals using a Landau-Ginzburg free energy expansion in the restricted temperature range $T_c - T \approx 5$ K. To extend the temperature range and to calculate these properties also for RbSCN, here we use a modified version of the compressible pseudospin model [34] by appending the free energy with gradient terms. The calculations are presented in the SM [49].

Figure 9 shows the resulting temperature dependence of the TB widths of RbSCN and KSCN as calculated in the SM [49]. Interestingly, the region of DW freezing appears for both crystals at a temperature where the TB width approaches a constant value of about 1–2 lattice constants. Similar behavior was found previously for domain freezing in KH_2PO_4 (KDP) (see Fig. 4 of Ref. [13]).

Inserting $w(T)$ and $\varepsilon_s(T)$ from the SM [49] into Eq. (6), we arrive at the temperature dependence of the critical stress $\sigma_c(T)$ shown in Fig. 8. Between room temperature and about 400 K, the critical stress σ_c varies only slightly, while between

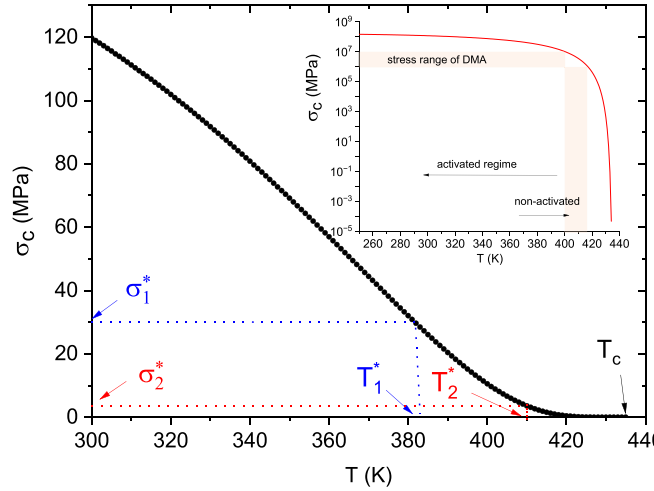


FIG. 8. Temperature dependence of the critical stress, which is necessary to unpin TBs in RbSCN. σ_1^* and T_1^* correspond to Fig. 6, and σ_2^* and T_2^* correspond to Fig. 5.

approximately 400 and 435 K it decreases by 10 orders of magnitude due to the exponential dependence on $w(T)$.

In the present DMA experiments the applied stress σ was in the range of 3–30 MPa. Thus, $\sigma < \sigma_c$ for temperatures below approximately 380 K. The following discussion relates to this activated temperature regime, in which only segments of TBs can be moved (thermally activated), thereby contributing to a TB-induced decrease of Y' and corresponding damping peaks in Y'' (and $\tan\delta$) below T^* (Figs. 4 and 5). According to [13], the DW contribution to the complex Young's modulus can be written as

$$Y(\omega) = Y^{\infty} - \frac{\Delta Y^{DW}}{1 + i\omega\tau_{\mathrm{DW}}}. \tag{7}$$

τ_{DW} is the characteristic time that it takes for a DW to settle into a new equilibrium position after being disturbed by an

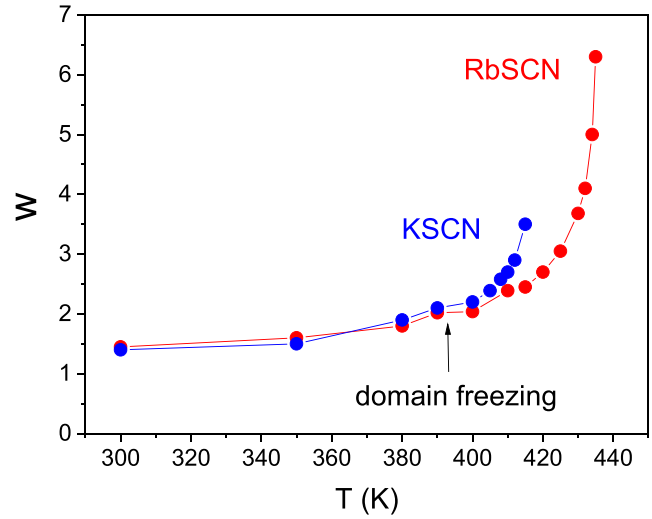


FIG. 9. Temperature dependence of the width w (in multiples of lattice constants) of twin boundaries of RbSCN and KSCN. Details of the calculation are given in the SM [49].

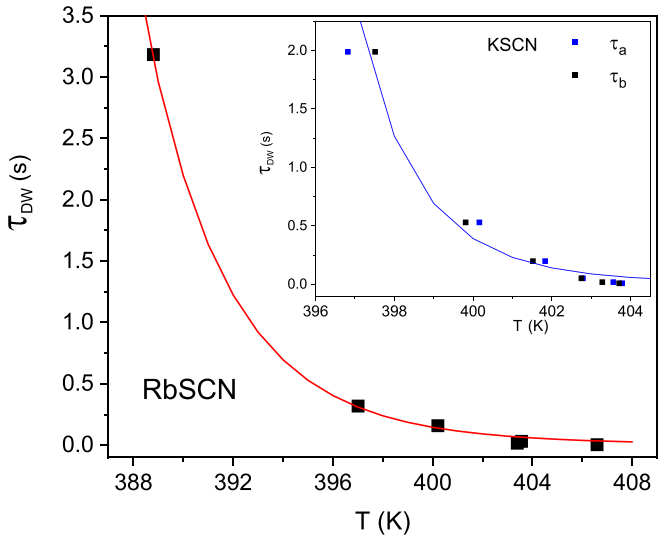


FIG. 10. Temperature dependence of the DW relaxation times of RbSCN and KSCN (inset). Points are determined from the peak shifts in Y'', the lines are fits using Eq. (11) with δ calculated in the SM [49], and the applied stress is $\sigma = 2$ MPa.

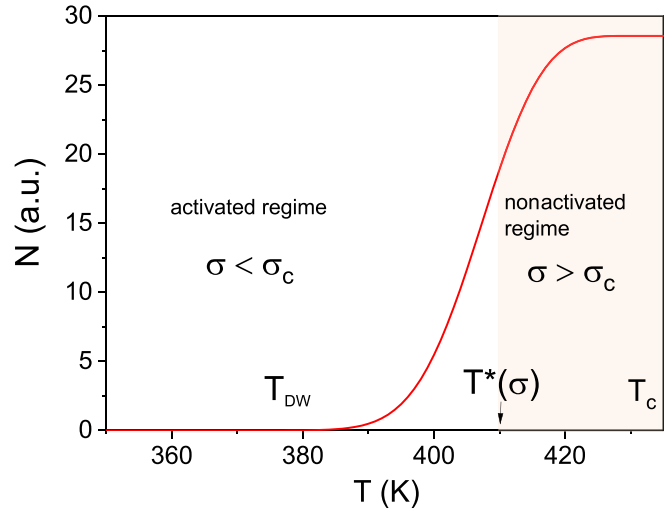


FIG. 11. Temperature dependence of the mean number N of inverse domain nuclei appearing per time unit of the unit area of a twin boundary in RbSCN, calculated from Eq. (12) with $\sigma = 4$ MPa.

external field (stress in the present case). The maxima of the damping peaks occur at a temperature T_{DW}, where $\omega\tau_{DW} = 1$. The shift of the maxima of the damping peaks with varying frequency (Figs. 4 and 5) is used to determine the DW relaxation time $\tau_{DW}(T)$. Adopting a simple Debye model, we can write

$$\tau_{DW}(T) = \tau_0 e^{\Pi^*/k_B T}, \tag{8}$$

where τ_0 is an effective attempt frequency and Π^* is the energy barrier for forming a critical nucleus of the switched domain segment [Fig. 7(a)]. In the simple approximation of a spherical nucleus of radius R, one obtains, for the energy of the nucleus of the other domain [54],

$$\Pi = \frac{2a}{\pi}\sqrt{2F_w(0)V_0}2\pi R - 2\varepsilon_s\sigma R^2\pi a. \tag{9}$$

The positive terms depending linearly on R originate from lattice pinning [55]. The negative term quadratic in R is the energy gain due to applied stress. Minimizing $\Pi(R)$ with respect to R (see also the SM [49]), one obtains the energy barrier Π^* for forming a critical nucleus of radius R^* as

$$\Pi^* = \frac{4aF_w(0)V_0}{\pi\varepsilon_s\sigma}. \tag{10}$$

Inserting Eq. (10) into Eq. (8), we get

$$\tau_{DW} = \tau_0 e^{\frac{4aF_w(0)V_0}{\pi\varepsilon_s\sigma k_B T}}. \tag{11}$$

Although we started from a simple Arrhenius relaxation time equation (8), according to Eq. (11), the DW relaxation time follows a double exponential temperature dependence since V_0 is already exponentially dependent on T.

Figure 10 shows the temperature dependences of the DW relaxation times of RbSCN and KSCN determined from the peaks in Y''. The double exponential law in Eq. (11) fits the data perfectly. This agreement with the data is even more remarkable, as Eq. (11) leaves, instead of the effective prefactor ($\tau_0 \approx 3 \times 10^{-2}$ s), no free parameters. All quantities entering Eq. (11), i.e., $F_w(0)$, V_0, and ε_s, are calculated from the compressible pseudospin model (see the SM [49]).

The mean number of other domain nuclei N appearing per time unit at the unit area of a TB increases exponentially with decreasing activation energy Π^* and thus takes the form [54] (see the SM [49])

$$N(T) \propto e^{-\Pi^*/k_B T}. \tag{12}$$

With increasing temperature, the number $N(T)$ of nuclei increases due to the decreasing Peierls potential [Eqs. (5) and (10)]. In the temperature range above approximately 380 K, $N(T)$ starts to increase substantially, simultaneously with the increase of the DW width (Fig. 9). At the temperature T^* one approaches the region where the applied stress σ starts to overcome the critical pinning stress σ_c. In the range $\sigma > \sigma_c$ (the nonactivated regime) an increasing number of TB segments in RbSCN become increasingly mobile (the DW relaxation time τ_{DW} is very small; Fig. 10) and these TB movements can trigger further events (Fig. 11) until large parts of the crystal have collectively switched.

As seen in Figs. 4 and 5, this switching results in a discontinuous increase in Y' and a corresponding peak in Y'' and $\tan\delta$ at T^*. In contrast to the damping peaks below T^*, these peaks do not shift with frequency. However, they do shift with applied stress. In the parallel plate experiment in Fig. 4 the applied force was approximately 8 N, whereas $F \approx 6$ N in the three-point bending experiment shown in Fig. 5, resulting in $T^*(\sigma) \approx 400$ K (Fig. 4) vs 410 K (Fig. 5). In Fig. 8 we show that the experimentally observed decrease of T^* with increasing stress fits perfectly with the calculation of the critical pinning stress $\sigma_c(T)$ using Eq. (6). In the experiment shown in Fig. 6 the initial heating run was performed to a temperature slightly above $T^* \approx 380$ K, followed by cooling back to room temperature and then heating again by crossing T_c. After cooling from $T \geqslant T^*$ all DW relaxation peaks disappeared,

implying that above $T^* \approx 380$ K, the crystal is indeed in a switched state.

V. SUMMARY AND CONCLUSION

The present dynamic elastic measurements of RbSCN in a broad range of temperatures (300–460 K) and frequencies (0.05–40 Hz and 100–600 kHz) and at various applied stresses yield insights into the rich dynamical behavior of twin boundaries. Ferroelastic domains either appear on cooling below $T_c \approx 435$ K and/or are already present in as-grown samples of RbSCN. The corresponding twin boundaries are oriented along (110) or $(\bar{1}10)$ planes. Due to the strain contrast between adjacent ferroelastic domains, the corresponding domain walls are mobile under dynamic stress applied in the a or b direction, which leads to superelastic softening in the corresponding Young's moduli Y'_{11} and Y'_{22} below T_c. The softening is accompanied by frequency-dependent peaks in Y''_{11} and Y''_{22}, shifting to lower temperatures with decreasing frequencies. The strong shift of these peaks, with maxima at $\omega\tau_{\mathrm{DW}} = 1$, is reflected in a sharp increase of the domain wall relaxation time τ_{DW} with decreasing temperature. A first attempt to fit the relaxation time using Arrhenius's law led to meaningless values of the preexponential factor and the activation energy. The Vogel-Fulcher law, with $\tau_{\mathrm{DW}} = \tau_0 \exp[E/k_B(T - T_{\mathrm{VF}})]$, fitted the data very well, with $\tau_0 \approx 10^{-5}$ s, $E \approx 0.037$ eV, and $T_{\mathrm{VF}} \approx 354$ K. In a recent work on KSCN [24], we also fitted the DW relaxation time by a Vogel-Fulcher law and obtained similar values, i.e., $\tau_0 \approx 10^{-7}$ s, $E \approx 0.035$ eV, and $T_{\mathrm{VF}} \approx 368$ K. These values are quite sound and may be related to jamming [56,57] as one of the prime mechanisms that generates glasslike states with glass freezing in crystals containing such high twin wall densities. The reason for Vogel-Fulcher-distributed dynamics may be due to the heterogeneous structure of the domain glass: Nucleation and propagation of domain walls see different energy barriers.

However, since the Vogel-Fulcher law is purely phenomenological, to get deeper insight into the microscopic mechanisms of TB motion in RbSCN, we adopted a Landau-Ginzburg type theory of thin domain walls [13,54]. Our calculations, based on a compressible pseudospin model, show that TBs in RbSCN and also in KSCN are, indeed, very thin (Fig. 9), with a nearly constant thickness of about 1–2 lattice constants from room temperature up to about 400 K. In this temperature range, the movement of the TBs in response to the applied dynamic stress occurs via thermally activated jumps of TB segments over energy barriers that are determined by the Peierls energy. This activation energy decreases exponentially with increasing TB width, which leads to a double exponential decrease of the DW relaxation time τ_{DW} with increasing temperature. Quite remarkably, Eq. (11) fits the experimental data on τ_{DW} perfectly (Fig. 10) without any free parameter. The movement of the thin TBs in the lattice relief occurs by thermally activated jumps up to a critical stress σ_c, which is also exponentially decreasing with increasing temperature (Fig. 8).

Around 400 K the critical stress σ_c starts to decrease by orders of magnitude due to an increase of the TB width. In this temperature region, the number of critical nuclei of the inverse domain increases enormously, and the applied stress starts to exceed σ_c. In this nonactivated regime, where the TBs are no longer pinned by the lattice potential, there appears to be a discontinuous increase of the Young's moduli in a and b directions around $T^*(\sigma) \approx 380$–410 K, accompanied by a peak in Y'' and $\tan\delta$. Heating RbSCN above about 380–410 K and cooling down again remove all signs of DW motion. This shows that, around the temperature $T^*(\sigma)$, the TB segments indeed become unpinned ($\sigma > \sigma_c$) and their mobility gets very high ($\tau_{\mathrm{DW}} < 0.1$ s), leading to a correlated avalanchelike switching of ferroelastic domains.

The question of why similar domain switching at T^* was not observed in recent experiments on the related crystal KSCN [24] arises, as there are no fundamental differences between RbSCN and KSCN. In both crystals the domain dynamics is mainly governed by thermally activated jumps of pinned domain wall segments over energy barriers that depend exponentially on DW thickness. Similar to RbSCN, the DW relaxation time of KSCN can also be fitted with a double exponential temperature dependence (inset of Fig. 10). However, unlike for RbSCN, we did not observe any stress-induced domain switching for KSCN for the following reasons: The stresses in three-point bending measurements of KSCN were generally lower (2–4 MPa) compared to those of RbSCN (4–30 MPa), and the critical stress needed to unpin the TBs in KSCN is a bit larger and approaches zero less steeply due to the fact that TBs in KSCN are thinner than those in RbSCN (Fig. 9). This shifts $T^*(\sigma)$ for KSCN very close to T_c, i.e., $T_c - T^* \approx 5$ K. At this temperature close to T_c, the effect of superelastic softening in Y' is already too small to allow for the observation of any detectable difference between a multidomain and a single-domain response.

Summarizing, we think that despite the simplifications made here, the present work gives valuable insights into the microscopic mechanisms of TB motion. In particular, the twin boundary thickness, its structure, and its temperature dependence seem to be key to explaining domain dynamics and domain freezing. Further work is needed to see to what extent the present physical insights can also be applied to other ferroelastic materials.

ACKNOWLEDGMENTS

This research was funded by the Austrian Science Fund (FWF), Grant DOIs: 10.55776/PIN2246224 and 10.55776/PAT2916124. RUS facilities in Cambridge were funded by the Natural Environment Research Council of United Kingdom (Grants No. NE/B505738/1 and No. NE/F017081/1). Part of this work was supported by the Czech Science Foundation (GACR), Project No. 25-18870L.

DATA AVAILABILITY

There are no publicly available research data or software supporting this manuscript. Requests for further information or data should be sent to the authors.

[1] E. K. H. Salje, *Phase Transitions in Ferroeleastic and Co-elastic Crystals* (Cambridge University Press, Cambridge,1993).

[2] P. Gao, J. Britson, C. T. Nelson, J. R. Jokisaari, C. Duan, M. Trassin, S.-H. Baek, H. Guo, L. Li, Y. Wang, Y.-H. Chu, A. M. Minor, C.-B. Eom, R. Ramesh, L.-Q. Chen, and X. Pan, Ferroelastic domain switching dynamics under electrical and mechanical excitations, Nat. Commun. **5**, 3801 (2014).

[3] G. Catalan, J. Seidel, R. Ramesh, and J. F. Scott, Domain wall nanoelectronics, Rev. Mod. Phys. **84**, 119 (2012).

[4] D. Meier, J. Seidel, M. Gregg, and R. Ramesh, *Domain Walls: From Fundamental Properties to Nanotechnology Concepts* (Oxford University Press, Oxford, 2020).

[5] R. J. Harrison and E. K. H. Salje, The noise of the needle avalanches of a single progressing needle domain in $LaAlO_3$, Appl. Phys. Lett. **97**, 021907 (2010).

[6] E. K. H. Salje, X. Ding, Z. Zhao, T. Lookman, and A. Saxena, Thermally activated avalanches: Jamming and the progression of needle domains, Phys. Rev. B **83**, 104109 (2011).

[7] S. Puchberger, V. Soprunyuk, W. Schranz, A. Tröster, K. Roleder, A. Majchrowski, M. A. Carpenter, and E. K. H. Salje, The noise of many needles, APL Mater. **5**, 046102 (2017).

[8] S. Puchberger, V. Soprunyuk, W. Schranz, and M. A. Carpenter, Segmental front line dynamics of randomly pinned ferroelastic domain walls, Phys. Rev. Mater. **2**, 013603 (2018).

[9] G. F. Nataf and E. K. H. Salje, Avalanches in ferroelectric, ferroelastic and coelastic materials: Phase transition, domain switching and propagation, Ferroelectrics **569**, 82 (2020).

[10] B. Casals, G. F. Nataf, and E. K. H. Salje, Avalanche criticality during ferroelectric/ferroelastic switching, Nat. Commun. **12**, 345 (2021).

[11] E. K. H. Salje, Ferroelastic materials, Annu. Rev. Mater. Res. **42**, 265 (2012).

[12] A. K. Tagantsev, L. E. Cross, and J. Fousek, *Domains in Ferroic Crystals and Thin Gilms* (Springer, New York, 2010).

[13] A. Sidorkin, Dynamics of domain walls in ferroelectrics and ferroelastics, Ferroelectrics **191**, 109 (1997).

[14] A. Bhattacharya and M. A. Zaeem, Mechanism of nucleation in ferroelastic domain switching, Scr. Mater. **252**, 116273 (2024).

[15] A. Bhattacharya and M. A. Zaeem, Kinetics of ferroelastic domain switching with and without back-switching events: A phase-field study, Acta Mater. **286**, 120702 (2025).

[16] G. Lu, S. Li, X. Ding, J. Sun, and E. K. H. Salje, Electrically driven ferroelastic domain walls, domain wall interactions, and moving needle domains, Phys. Rev. Mater. **3**, 114405 (2019).

[17] X. He, S. Li, X. Ding, J. Sun, S. Kustov, and E. K. H. Salje, Internal friction in complex ferroelastic twin patterns, Acta Mater. **228**, 117787 (2022).

[18] H. Barkhausen, Zwei mit hilfe der neuen Verstärker entdeckte Erscheinugen, Z. Phys. **20**, 401 (1919).

[19] S. Zapperi, P. Cizeau, G. Durin, and H. E. Stanley, Dynamics of a ferromagnetic domain wall: Avalanches, depinning transition, and the Barkhausen effect, Phys. Rev. B **58**, 6353 (1998).

[20] P. Paruch and J. Guyonnet, Nanoscale studies of ferroelectric domain walls as pinned elastic interfaces, C. R. Phys. **14**, 667 (2013).

[21] S. Lemerle, J. Ferré, C. Chappert, V. Mathet, T. Giamarchi, and P. Le Doussal, Domain wall creep in an Ising ultrathin magnetic film, Phys. Rev. Lett. **80**, 849 (1998).

[22] W. Kleemann, Universal domain wall dynamics in disordered ferroic materials, Annu. Rev. Mater. Res. **37**, 415 (2007).

[23] A. Shlyaykher, T. Pippinger, T. Schleid, O. Reckeweg, and F. Tambornino, Syntheses, crystallographic characterization, and structural relations of Rb[SCN], Z. Kristallogr. - Cryst. Mater. **237**, 69 (2022).

[24] V. Soprunyuk, P. König, A. Tröster, W. Schranz, M. A. Carpenter, and E. K. H. Salje, Domain glass dynamics of potassium thiocyanate KSCN, J. Appl. Phys. **137**, 145101 (2025).

[25] Y. Yamada and T. Watanabe, The phase transition of crystalline potassium thiocyanate, KSCN. II. X-ray study, Bull. Chem. Soc. Jpn. **36**, 1032 (1963).

[26] S. Yamamoto, M. Sakuno, and Y. Shinnaka, Structure analysis of the phase transition in KSCN, J. Phys. Soc. Jpn. **56**, 4393 (1987).

[27] V. Janovec, W. Schranz, H. Warhanek, and Z. Zikmund, Symmetry analysis of domain structure in KSCN crystals, Ferroelectrics **98**, 171 (1989).

[28] W. Schranz, I. Rychetsky, and J. Hlinka, Polarity of domain boundaries in nonpolar materials derived from order parameter and layer group symmetry, Phys. Rev. B **100**, 184105 (2019).

[29] R. Blinc, J. Seliger, T. Apih, J. Dolinsek, A. Fuith, W. Schranz, and H. Warhanek, ^{87}Rb NMR of the structural phase transition in RbSCN, Phys. Rev. B **52**, 833 (1995).

[30] O. Blaschko, W. Schwarz, W. Schranz, and A. Fuith, Domain formation in the order-disorder phase transition of RbSCN, J. Phys.: Condens. Matter **6**, 3469 (1994).

[31] S. Sathaiah and H. D. Bist, Structural phase transition and internal fields in rubidium thiocyanate probed through vibrational spectroscopy, Z. Phys. B **84**, 423 (1991).

[32] M. M. Ossowski, J. R. Hardy, and R. W. Smith, Molecular-dynamics of phase transitions in alkali thiocyanates, Phys. Rev. B **62**, 3136 (2000).

[33] Z. Lodziana, W. Schranz, and A. Fuith, Monte Carlo simulations of the pseudospin model of RbSCN, J. Phys.: Condens. Matter **11**, 2449 (1999).

[34] W. Schranz, H. Warhanek, R. Blinc, and B. Zeks, Pseudospin model for KSCN, Phys. Rev. B **40**, 7141 (1989).

[35] W. Schranz, Static and dynamic properties of the order-disorder phase transition in KSCN and related crystals, Phase Transitions **51**, 1 (1994).

[36] W. Schranz and D. Havlik, Heat-diffusion central peak in the elastic susceptibility of KSCN, Phys. Rev. Lett. **73**, 2575 (1994).

[37] W. Schranz, A. Fuith, A. Tröster, and J. Kroupa, Dynamic acoustic anomalies in KSCN near the improper ferroelastic phase transition, Ferroelectrics **314**, 189 (2005).

[38] R. Blinc, J. Seliger, T. Apih, J. Dolinšek, I. Zupančič, O. Plyushch, A. Fuith, W. Schranz, H. Warhanek, B. Topič, and U. Haeberlen, ^{39}K NMR study of the antiferroelectric phase transition in potassium thiocyanate, Phys. Rev. B **43**, 569 (1991).

[39] O. Blaschko, W. Schwarz, W. Schranz, and A. Fuith, Order-disorder phase transition in potassium thiocyanate, Phys. Rev. B **44**, 9159 (1991).

[40] O. Blaschko, W. Schranz, M. Fally, G. Krexner, and Z. Lodziana, Strain-stabilized precursor clusters in potassium thiocyanate, Phys. Rev. B **58**, 8362 (1998).

[41] K. Parlinski, Computer simulation of domain formation in the order-disorder phase transition of the KSCN model, Phys. Rev. B **50**, 59 (1994).

[42] Z. Lodziana and K. Parlński, Computer simulation of diffuse scattering from KSCN crystal, Phase Transitions **58**, 273 (1996).
[43] A. Tröster, W. Schranz, G. Krexner, A. V. Kityk, and Z. Lodziana, Suppression of the order parameter correlation length by inhomogeneous strains, Phys. Rev. Lett. **85**, 2765 (2000).
[44] A. Tröster *et al.* MC simulations of a compressible pseudospin model including inhomogeneous strains (unpublished).
[45] A. Fuith, The KSCN family: Structural properties and phase transitions of crystals with three-atomic linear anions, Phase Transitions **62**, 1 (1997).
[46] R. E. A. McKnight, T. Moxon, A. Buckley, P. A. Taylor, T. W. Darling, and M. A. Carpenter, Grain size dependence of elastic anomalies accompanying the $\alpha - \beta$ phase transition in polycrystalline quartz, J. Phys.: Condens. Matter **20**, 075229 (2008).
[47] W. Schranz, Superelastic softening in perovskites, Phys. Rev. B **83**, 094120 (2011).
[48] W. Schranz, H. Kabelka, A. Sarras, and M. Burock, Giant domain wall response of highly twinned ferroelastic materials, Appl. Phys. Lett. **101**, 141913 (2012).
[49] See Supplemental Material at http://link.aps.org/supplemental/10.1103/rmsb-fvm3 for details of the theory of domain wall dynamics and the Landau-Ginzburg free energy of RbSCN, which is used to calculate the properties of the antiphase boundaries and twin boundaries of RbSCN, which includes Refs. [58–61].
[50] R. J. Harrison, S. A. T. Redfern, and E. K. H. Salje, Dynamical excitation and anelastic relaxation of ferroelastic domain walls in $LaAlO_3$, Phys. Rev. B **69**, 144101 (2004).
[51] S. Puchberger, V. Soprunyuk, A. Majchrowski, K. Roleder, and W. Schranz, Domain wall motion and precursor dynamics in $PbZrO_3$, Phys. Rev. B **94**, 214101 (2016).
[52] A. V. Kityk, W. Schranz, P. Sondergeld, D. Havlik, E. K. H. Salje, and J. F. Scott, Low frequency superelasticity and non linear elastic behavior of $SrTiO_3$ crystals, Phys. Rev. B **61**, 946 (2000).
[53] I. Rychetsky and W. Schranz, Ferroelastic domain walls in Hg_2Br_2 and KSCN, J. Phys.: Condens. Matter **6**, 11159 (1994).
[54] A. S. Sidorkin, Domain boundaries in ferroelectrics, J. Adv. Dielectr. **02**, 1230013 (2012).
[55] B. M. Darinskii and A. S. Sidorkin, The motion of the domain boundaries in crystals of KH_2PO_4 group, Ferroelectrics **71**, 269 (1987).
[56] E. K. H. Salje, X. Ding, and O. Aktas, Domain glass, Phys. Status Solidi B **251**, 2061 (2014).
[57] E. K. H. Salje and M. A. Carpenter, Domain glasses: Twin planes, Bloch lines, and Bloch points, Phys. Status Solidi B **252**, 2639 (2015).
[58] J. Kroupa, J. Fousek, A. Fousková, J. Petzelt, M. Pavel, S. Kamba, and H. H. Warhanek, New data on the phase transition in KSCN, Ferroelectrics **87**, 121 (1988).
[59] I. Rychetsky and W. Schranz, Antiphase boundaries in Hg_2Br_2 and KSCN, J. Phys.: Condens. Matter **5**, 1455 (1993).
[60] G. Blatter, M. V. Feigelman, V. B. Geshkenbein, A. I. Larkin, and V. M. Vinokur, Vortices in high-temperature superconductors, Rev. Mod. Phys. **66**, 1125 (1994).
[61] E. A. H. Love, *A Treatise on the Mathematical Theory of Elasticity* (Dover, New York, 1944), p. 49.